AGU PUBLICATIONS

JGR

Journal of Geophysical Research: Atmospheres

RESEARCH ARTICLE
10.1002/2015JD023950

Key Points:
- AIRS and MODIS ice cloud properties are very consistent in homogeneous clouds
- Nearly perfect agreement in optical thickness in single-layered, low-latitude ice clouds
- Systematic bias of 5–10 μm remains in effective radius

Correspondence to:
B. H. Kahn,
brian.h.kahn@jpl.nasa.gov

Citation:
Kahn, B. H., M. M. Schreier, Q. Yue, E. J. Fetzer, F. W. Irion, S. Platnick, C. Wang, S. L. Nasiri, and T. S. L'Ecuyer (2015), Pixel-scale assessment and uncertainty analysis of AIRS and MODIS ice cloud optical thickness and effective radius, *J. Geophys. Res. Atmos.*, *120*, 11,669–11,689, doi:10.1002/2015JD023950.

Received 16 JUL 2015
Accepted 3 NOV 2015
Accepted article online 4 NOV 2015
Published online 25 NOV 2015

Pixel-scale assessment and uncertainty analysis of AIRS and MODIS ice cloud optical thickness and effective radius

B. H. Kahn[1], M. M. Schreier[1], Q. Yue[1], E. J. Fetzer[1], F. W. Irion[1], S. Platnick[2], C. Wang[2], S. L. Nasiri[3], and T. S. L'Ecuyer[4]

[1]Jet Propulsion Laboratory, California Institute of Technology, Pasadena, California, USA, [2]NASA Goddard Space Flight Center, Greenbelt, Maryland, USA, [3]Department of Atmospheric Sciences, Texas A&M University, College Station, Texas, USA, [4]Department of Atmospheric and Oceanic Sciences, University of Wisconsin-Madison, Madison, Wisconsin, USA

Abstract Comparisons of collocated Atmospheric Infrared Sounder (AIRS) and Moderate Resolution Imaging Spectroradiometer (MODIS) ice cloud optical thickness (τ) and effective radius (r_e) retrievals and their uncertainty estimates are described at the pixel scale. While an estimated 27% of all AIRS fields of view contain ice cloud, only 7% contain spatially uniform ice according to the MODIS 1 km optical property phase mask. The ice cloud comparisons are partitioned by horizontal variability in cloud amount, cloud top thermodynamic phase, vertical layering of clouds, and other parameters. The magnitudes of τ and r_e and their relative uncertainties are compared for a wide variety of pixel-scale cloud complexity. The correlations of τ and r_e between the two instruments are strong functions of horizontal cloud heterogeneity and vertical cloud structure, with the highest correlations found in single-layer, horizontally homogeneous clouds over the low-latitude tropical oceans. While the τ comparisons are essentially unbiased for homogeneous ice cloud with variability that depends on scene complexity, a bias of 5–10 μm remains in r_e within the most homogeneous scenes identified, consistent with known radiative transfer differences in the visible and infrared bands. The AIRS and MODIS uncertainty estimates reflect the wide variety of cloud complexity, with greater magnitudes in scenes with larger horizontal variability. The AIRS averaging kernels suggest scene-dependent information content that is consistent with infrared sensitivity to ice clouds. The AIRS-normalized χ^2 radiance fits suggest that accounting for horizontal cloud variability is likely to improve the AIRS ice cloud retrievals.

1. Introduction

Clouds and their associated processes are the largest sources of uncertainty in future climate model projections [*Intergovernmental Panel on Climate Change*, 2013]. A significant number of decadal-scale or longer satellite remote sensing data sets of cloud properties are now publicly available and are actively used in climate research. Ongoing efforts to resolve discrepancies among these cloud observational records have been successful yet incremental and, to a large degree, are explained by differences in instrument characteristics and their dependencies on different types of hydrometeors, retrieval algorithm assumptions and methodologies, spatial resolution, and temporal sampling characteristics [*Stubenrauch et al.*, 2013]. While the interconsistency of satellite-based estimates of cloud amount, cloud top height/temperature, and effective emissivity are generally understood [e.g., *Rossow et al.*, 1985; *Menzel et al.*, 2008; *Nasiri et al.*, 2011], the wide spread in estimates of cloud thermodynamic phase among active and passive sensors [*Nasiri and Kahn*, 2008; *Cho et al.*, 2009; *Hu et al.*, 2009; *Riedi et al.*, 2010] and ice cloud optical thickness and effective radius [e.g., *Davis et al.*, 2009; *Zhang et al.*, 2010; *Stein et al.*, 2011; *Deng et al.*, 2013; *Stubenrauch et al.*, 2013] remain poorly understood.

Recent advances in the parameterization of microphysical processes in climate models highlight a need for additional observational constraints of ice cloud microphysics [*Hendricks et al.*, 2011; *Gettelman et al.*, 2010] and cloud thermodynamic phase [*Tsushima et al.*, 2006; *Cheng et al.*, 2012; *Storelvmo et al.*, 2011; *Cesana et al.*, 2012]. Climate models are very sensitive to the formulation of the subgrid ice microphysical parameterizations [e.g., *Mitchell et al.*, 2008; *Barahona et al.*, 2010; *Gettelman et al.*, 2010; *Lohmann and Karcher*, 2002]. Well-characterized ice microphysical observations with quantitative error estimates are necessary for the assessment and improvement of the models [*Waliser et al.*, 2009]. At present, it remains unclear if the currently available remote sensing observations are capable of this.

Previous studies have demonstrated that a multisensor retrieval approach developed from a combination of active and passive sensors such as those available on NASA's A-Train and to be available from the Earth Clouds, Aerosol and Radiation Explorer (EarthCare) [*European Space Agency*, 2004] will significantly improve ice cloud microphysical and optical property retrievals [e.g., *Miller et al*., 2000; *Delanoë and Hogan*, 2008; *Deng et al*., 2013]. *Cooper et al.* [2003] showed that cloud boundary information from active sensors improves ice cloud optical thickness (τ) retrievals derived from the mid-infrared (MIR). *Delanoë and Hogan* [2008, 2010], *Cooper et al.* [2006, 2007], and many additional studies have clearly demonstrated that the practical development of synergistic, multichannel, multisensor retrievals requires a thorough and quantitative understanding of individual sensor information content and retrieval performance. Toward this end, ongoing validation and intercomparisons of existing single-sensor ice cloud retrieval records are useful for determining the types of cloud configurations that are candidates for improvements within a multisensor cloud retrieval.

Zhang et al. [2010] showed that the vertical inhomogeneities of ice particle size and ice water content are a source of potentially significant τ-dependent differences between ice cloud effective radius (r_e) retrievals using sets of channels in the visible and near-infrared (VNIR) and the MIR. Furthermore, *Zhang et al.* [2010] found that VNIR-derived r_e may be several microns greater than MIR-derived r_e because of the nonlinear dependence of single-scattering albedo and extinction on r_e, yet both sets of spectral bands may underestimate the true value of r_e.

Hyperspectral MIR observations have shown potential for higher-quality retrievals of ice cloud microphysics in transparent cirrus and cloud top thermodynamic phase, when compared to coarser resolution MIR narrowband measurements [*Chung et al*., 2000; *Wei et al*., 2004; *Nasiri and Kahn*, 2008; *Guignard et al*., 2012; *Wang et al*., 2013]. This work attempts to glean further insight on the relative strengths and weaknesses of high-spectral-resolution MIR sounder and high-spatial-resolution narrowband VNIR imager retrievals of ice cloud properties. The ice cloud τ and r_e obtained from the Earth Observing System Aqua Atmospheric Infrared Sounder (AIRS) version 6 (V6) release [*Kahn et al*., 2014, abbreviated as *K14*] and the Moderate Resolution Imaging Spectroradiometer (MODIS) collection 6 (C6) release [e.g., *Baum et al*., 2012; *Platnick et al*., 2014] are separately compared across a variety of complex cloud configurations. The cloud top thermodynamic phase and ice cloud property retrievals are a new component of the AIRS V6 operational product release. The equivalent cloud top properties from the MODIS Science Team algorithm have been refined and improved over multiple data collections [*Platnick et al*., 2003] with collection 6 containing improvements that are specific to ice cloud top properties [*Platnick et al*., 2014]. The Aqua MODIS and AIRS instruments have observed Earth simultaneously and nearly continuously since launch on 4 May 2002. We anticipate that this comparison will serve as a useful benchmark for ice cloud observational records obtained from the Visible Infrared Imaging Radiometer Suite (VIIRS) and Cross-track Infrared Sounder (CrIS) instruments on Suomi NPP and the future Joint Polar Satellite Systems.

There are unresolved questions about the consistencies of AIRS and MODIS ice cloud property retrievals and how they should be utilized in research efforts. Toward this end, our specific focus is on the comparison of AIRS and MODIS ice cloud properties that are "built up" from pixel resolution level 2 (L2) retrievals. The collocated observations are stratified by horizontal cloud heterogeneity, the occurrence of single-layer or multilayer clouds, AIRS and MODIS estimates of cloud thermodynamic phase, surface type, latitude, solar zenith angle, and reported uncertainty estimates. A comparison of cloud properties at the native sensor resolution and sampling is the best choice to minimize the ambiguity of comparisons that increases with spatial and temporal averaging over cloud types, scene complexity, and stratification from other geophysical variables. We will show that the stratification of the observational comparisons confirms results inferred from narrowband VNIR and MIR radiative transfer calculations of ice clouds [*Zhang et al*., 2010], leads to new insights on the optimal use of currently available single-sensor MODIS and AIRS ice cloud retrievals and their reported uncertainties, and helps to clarify the path forward on the development of combined multisensor imager and sounder ice cloud retrievals.

2. Data and Methodology

The AIRS V6 cloud thermodynamic phase retrieval is described at length in *K14* and validated against Cloud-Aerosol Lidar with Orthogonal Polarization (CALIOP) in *Jin and Nasiri* [2014]. A set of four brightness

Table 1. Breakdown of the Individual Ice Phase Tests That Are Summed Into a Single Value for the "Phase Test" (+1 to +4) Presented in This Work[a]

Description	Channels and Thresholds	Features	Value
Cold ice cloud test	T_b 960 cm^{-1} < 235 K	Cold and opaque ice cloud detection	+1
Particle scattering test	ΔT_b 1231–960 cm^{-1} > 0.0 K	Ice and liquid discrimination	+1
Thin cirrus test	ΔT_b 1231–930 cm^{-1} > 1.75 K	Thin cirrus identification	+1
Water vapor line test	ΔT_b 1227–960 cm^{-1} > −0.5 K	Discriminate cirrus from water vapor	+1

[a]There is no relationship between the number of positive ice phase tests triggered and the definition of the four heterogeneity categories defined in Table 2.

temperature (T_b) thresholds and T_b differences (ΔT_b) in the 8–12 μm atmospheric window region are used to identify the presence of ice cloud (Table 1) that leverages the spectral dependencies of the refractive indices of ice and liquid water [*Nasiri and Kahn*, 2008]. Convective clouds generally have larger values of τ and pass more of the ice phase tests, while stratiform clouds have smaller values of τ and pass fewer tests [*K14*; *Naud and Kahn*, 2015]. About 99% of AIRS fields of view (FOVs) that are identified as single-layered ice clouds have at least a portion of the FOV covered with ice according to the CALIOP phase feature mask [*Jin and Nasiri*, 2014]. This value is reduced to 94% and 96% for multilayer and horizontally heterogeneous clouds, respectively. *Jin and Nasiri* [2014] show that horizontally heterogeneous cloud contains a high proportion of phase mixtures within the AIRS FOV according to CALIOP. Consequently, the AIRS thermodynamic phase algorithm is considered to be a very sensitive ice cloud detector in cases of either uniform or heterogeneous FOVs but a much less sensitive liquid cloud detector especially in broken clouds (*K14*).

The AIRS V6 ice cloud retrieval (*K14*) is based on an optimal estimation methodology [*Rodgers*, 2000]. The retrieval state vector is restricted to τ (*ice_cld_opt_depth*), r_e (*ice_cld_eff_diam*; D_e is converted to r_e), and ice cloud top temperature $T_{c,ice}$ (*ice_cld_temp_eff*) so as to (1) maximize computational efficiency and (2) exploit the available AIRS L2 retrievals produced by the cloud-clearing algorithm. Uncertainty estimates are reported for the three state vector retrieval parameters. The AIRS Standard L2 products are used as fixed priors (temperature and water vapor profiles and surface temperature and emissivity), constraints, and initial guesses (e.g., the upper cloud top temperature is used as the first guess for $T_{c,ice}$). Scalar averaging kernels (AKs) and a normalized chi-squared (χ^2) fitting parameter between nearly 60 observed and simulated channels (*K14*) are reported. Values of AKs approaching 1.0 suggest that the observations contain relatively high values of information content, while values of χ^2 near 1.0 suggest good fits between simulated and observed radiances. Lower values of AKs suggest reduced information content while higher values of χ^2 indicate poorer spectral fits; the full range of scene complexity is not accounted for in the simulated radiances.

The updated MODIS collection 6 (C6) cloud thermodynamic phase and cloud optical properties are described in *Platnick et al.* [2014]. The MODIS 1 km cloud mask [*Frey et al.*, 2008] identifies cloudy pixels as *confident cloudy* or *probably cloudy* and is used to derive cloud optical thickness (τ) and effective radius (r_e). There are three separate r_e retrievals that are based on absorption coefficient differences of ice in three shortwave infrared bands centered at 1.6, 2.1, and 3.7 μm [*Nakajima and King*, 1990]. Three separate cloud thermodynamic phase products are made available: a 5 km MIR phase mask, a 1 km MIR phase mask, and a combined 1 km VNIR and MIR operational phase mask. The latter is used for the cloud optical property retrievals and determines whether ice or liquid water cloud look-up tables are used in the retrieval. C6 improvements in the cloud optical property phase mask have led to improved detection in broken clouds and near the edges of thin cirrus clouds [*Platnick et al.*, 2014]. In addition to the standard retrievals, C6 also includes partly cloudy retrievals for broken/near-edge ice cloud pixels; however, partly cloudy pixels have been excluded from this analysis. Pixel-level uncertainty estimates are available for the cloud optical property retrievals by calculating Jacobians from precomputed look-up tables and propagating measured and model uncertainty components into retrieval uncertainty space [*Platnick et al.*, 2014]. Furthermore, multilayer clouds [*Wind et al.*, 2010] are detected and reported along with a pseudo confidence level that is a weighted sum of individual tests used in the algorithm (see Table 2.10.1-1 in *Platnick et al.* [2014]).

In this study all available daytime MODIS C6 cloud observations from 1 to 31 May 2012 are collocated within coincident AIRS footprints (~13.5 km at nadir) using the smeared, truncated, and rotated spatial response functions described in *Schreier et al.* [2010]. We average all MODIS τ and r_e retrievals within the AIRS footprint and then stratify the observations by metrics of cloud complexity. We use two independent metrics that determine the existence of multiple-layer clouds. First, values of the MODIS multilayer flag are averaged over

Table 2. Definitions for AIRS Footprint Cloud Heterogeneity Using the 1 km MODIS VNIR Optical Property Cloud Thermodynamic Phase[a]

Label	Description	VNIR Cloud Mask	Phase	Percent of FOVs (τ)	Number of FOVs (τ)
HOM	Homogeneous ice	100%	Ice only	6.7%	3.03×10^6
HET	Heterogeneous ice	<100%	Ice only	1.2%	5.42×10^5
MIX	Heterogeneous or homogeneous ice and liquid	≤100%	Ice and liquid	11.1%	5.02×10^6
DIFF	Heterogeneous or homogeneous liquid	≤100%	Liquid only	0.8%	3.62×10^5

[a]Percentages and counts are defined for the τ comparisons.

all cloudy pixels and "single-layer" clouds are defined by requiring the averaged multilayer flag value in the AIRS FOV < 1.5. Second, the AIRS lower layer effective cloud fraction (ECF) < 0.1 is also required to meet the criterion of a single-layer cloud. These delineations are arbitrary but were chosen in order to reduce the sample size similarly for both metrics.

Horizontal heterogeneity in thermodynamic phase is determined from the MODIS 1 km VNIR optical property phase mask. The horizontal cloud heterogeneity within the AIRS FOV that contains ice according to AIRS ice tests is divided into four general categories (Table 2) and is similar to the approach taken in *Kahn et al.* [2011]: 100% homogeneous ice cloud coverage according to MODIS (HOM), less than 100% ice cloud coverage but no liquid cloud according to MODIS (HET), up to and including 100% cloud coverage with a least one 1 km pixel each of liquid and ice according to MODIS (MIX), and up to and including 100% liquid cloud coverage but no ice according to MODIS (DIFF).

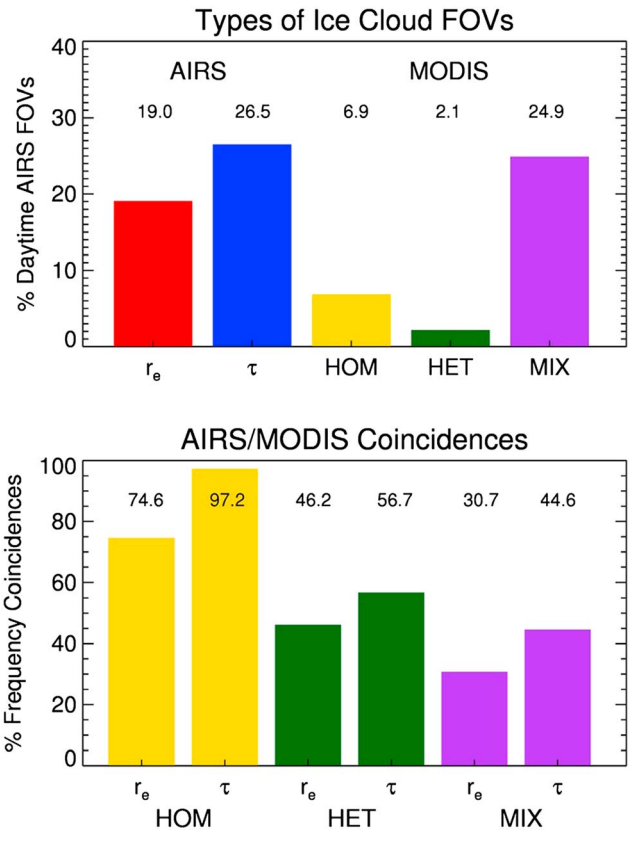

Figure 1. (top) The frequencies of AIRS τ and r_e retrievals and the types of MODIS retrievals that are averaged within the AIRS FOV are shown. See Table 1 for definitions of HOM, HET, and MIX. (bottom) The frequencies of AIRS and MODIS τ and r_e retrieval coincidences for the HOM, HET, and MIX categories in percent are shown. Note that these percentages are of the AIRS and MODIS coincidences shown in the top plot.

All of the τ and r_e retrievals are averaged with equal pixel weighting over the cloudy MODIS pixels. Once the scene heterogeneity is determined within each AIRS FOV, the matched AIRS and MODIS data are categorized into separate histograms of τ and r_e. The Pearson's correlation coefficient, the Spearman's ranked correlation coefficient (ρ), and the percentage of the sample size to the total available data (N) are reported.

3. MODIS Cloud Heterogeneity Within the AIRS Footprint

Over the lifetime of the AIRS mission approximately 27% of all AIRS FOVs contain ice [*Liou*, 1986] according to ice tests in the *cld_phase_bits* field reported in the AIRS Support L2 product, and the ice cloud fraction is 26.5% for the 1 month period (May 2012) considered in this work. The occurrence frequencies of valid ice cloud τ and r_e retrievals and the occurrence frequencies of MODIS cloud thermodynamic phase mixtures within the AIRS FOV are shown in Figure 1. According to the MODIS VNIR phase mask, 11.1% of AIRS FOVs are categorized as MIX (liquid and ice). About 6.7% of AIRS FOVs are categorized as HOM (uniform ice), while about 1.2% are categorized as HET (broken ice).

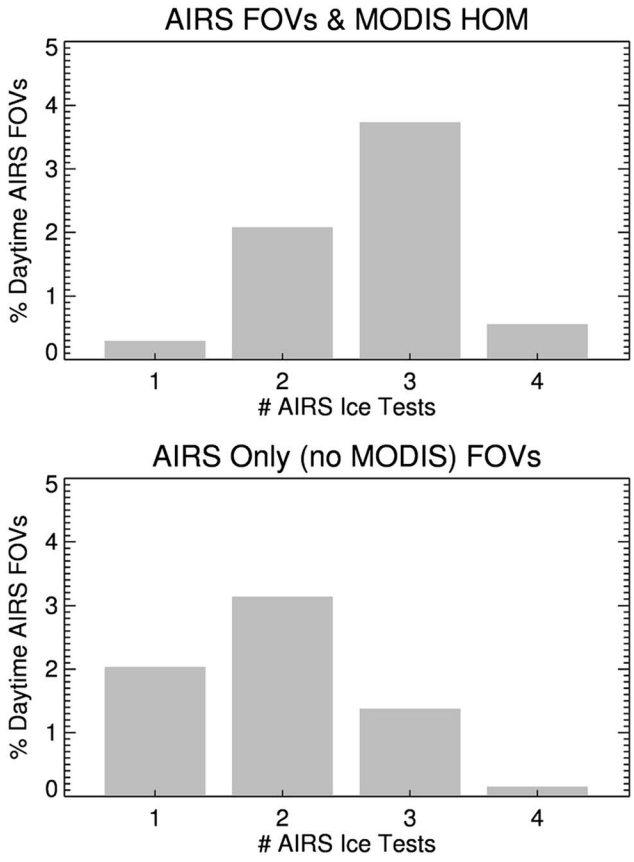

Figure 2. (top) The frequency of occurrence of the number of positive ice tests (1 to 4) that occur when coinciding AIRS and MODIS τ retrievals in HOM scenes is shown. (bottom) The frequency of occurrence of the number of positive ice tests (1 to 4) that occur when AIRS reports a value of τ while MODIS reports clear sky according to the 1 km cloud mask is shown.

Therefore, over half (19.0% out of the 26.5%) of the ice-containing AIRS FOVs have at least some ice according to the MODIS VNIR phase mask. The remaining 7.5% of AIRS FOVs that contain ice are almost always clear according to the VNIR phase mask and is a strong indication that AIRS detects a significant portion of thin cirrus [*Kahn et al.*, 2008]. However, a small percentage of ice-containing AIRS FOVs (<1%) have either heterogeneous or homogeneous liquid phase clouds according to the VNIR phase mask (not shown in Figure 1). These percentages change if the VNIR phase mask is replaced with the 1 km or 5 km MIR phase masks, but the overall comparisons within each categorization are very similar (not shown).

Nearly all AIRS FOVs that contain ice have valid τ retrievals (26.5%), while only ~72% of these τ retrievals have valid r_e retrievals (19.0%). The discrepancy is a result of the criteria used to define the quality control (QC) flags that mimic the temperature or water vapor profile QC in the AIRS Standard L2 retrievals (*K14*). A more stringent QC that was designed for r_e successfully filters out a number of noisy values of r_e but at the cost of removing 28% of all r_e retrievals. The noise in r_e is traced to the existence of subtle spectral signatures in the 8–12 μm window that arise from heterogeneous and multilayered clouds in the AIRS FOV, and possible improvements in the retrieval are a subject of ongoing research.

The ratio of valid r_e retrievals to valid τ retrievals is similar between HOM and HET (Figure 1, bottom). However, the ratio for MIX is reduced compared to HET and HOM and indicates that a higher proportion of r_e retrievals failed the QC criteria. This is an encouraging result when one considers the degree of cloud complexity in the MIX FOVs that (1) have measurably reduced magnitudes of information content evidenced by lower values of the scalar averaging kernel (AK) for r_e (to be shown) and (2) poorer spectral fits between the simulated and observed radiances that are reflected in higher values of χ^2 (see Appendix A). Therefore, we argue that the reduction of valid r_e retrievals in complex cloud configurations lends confidence to the AIRS operational retrieval approach (*K14*) and suggests that a combined AIRS and MODIS ice cloud retrieval algorithm may help characterize these complex clouds.

Figure 2 shows the breakdown of the number of positive ice phase tests for HOM and the remaining 7.5% of AIRS FOVs that contain ice according to AIRS (but not according to the MODIS VNIR phase mask). The number of positive tests is on average higher for HOM, while ice detected only by AIRS usually passes just one or two positive tests. This is further confirmation that AIRS detects some cirrus when the operational MODIS cloud mask does not [*Ackerman et al.*, 2008].

To relate spatial patterns between the ice phase tests and the retrieved ice cloud properties, global distributions of ice phase frequency organized by the number of passed ice phase tests are shown in Figure 3. The frequency of one and two positive tests is higher in the midlatitude storm tracks and over land especially near

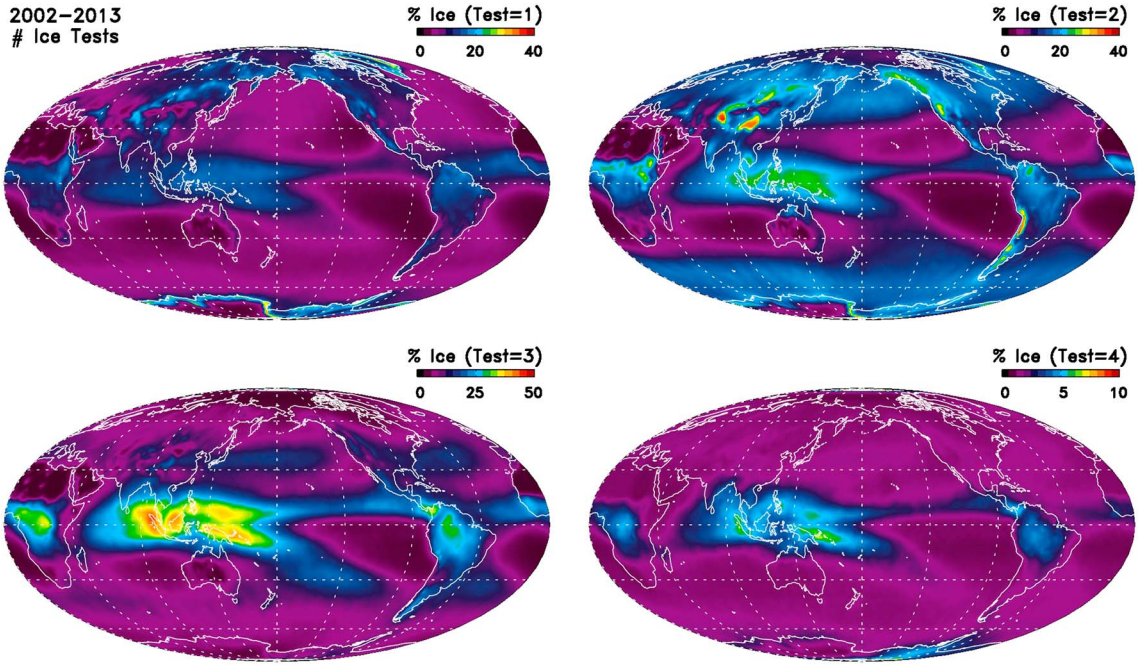

Figure 3. Frequency of occurrence of ice clouds for the total number of positive AIRS cloud thermodynamic ice phase tests. The maximum value of any grid box cannot exceed 100% when summing all four categories.

topographic features. While many of the clouds over land are associated with orographic ice clouds, there are inevitably some false positive tests that result from unresolved spatial heterogeneity in surface emissivity and temperature. For three and four positive phase tests, the patterns of subtropical and tropical thin cirrus and deep convection over tropical land emerge.

Global distributions of τ grouped by the number of positive ice phase tests are shown in Figure 4. As expected, the lowest values of τ coincide with one positive test. These clouds are predominantly thin cirrus in the tropics with a reduced occurrence frequency over midlatitude landmasses and polar latitudes (see Figure 3). Interestingly, one positive test also coincides with optically thick ice cloud in the potentially mixed-phase temperature range (250–265 K) located in the cold sector of midlatitude cyclones that are described by *Naud and Kahn* [2015]. For two positive tests, a similar pattern as in one positive test is found but with an upward shift in τ for tropical cirrus and a shift to stratiform warm frontal clouds from cold sector clouds in midlatitude cyclones [*Naud and Kahn*, 2015]. For three positive tests, τ is higher nearly everywhere compared to one or two positive tests especially in the tropics and the more convectively unstable areas of the warm sector in midlatitude cyclones [*Naud and Kahn*, 2015]. In the storm tracks, higher values of τ are found in the western ocean basins where cyclogenesis is most common [*Hoskins and Hodges*, 2002]. For four positive tests, an approximately zonal symmetric pattern emerges and is similar to MODIS ice cloud τ distributions described in *King et al.* [2013]. This result is encouraging as it demonstrates the overlapping sensitivity of subsets of AIRS and MODIS ice cloud properties for thicker ice clouds.

Global distributions of r_e stratified by the number of positive ice phase tests are shown in Figure 5. For one positive test, small values of r_e spatially coincide with low values of τ in tropical thin cirrus, in particular where cloud top temperatures are coldest (*K14*). Higher values of r_e are shifted equatorward relative to the latitude where maximum values of τ are found within the storm track. This shift is clearly observed in midlatitude cyclone composites, and the southward location of larger ice particles is consistent with warmer, moister, and convectively unstable air masses that lead to large particles from convective lofting [*Naud and Kahn*, 2015]. For two positive tests, the patterns are similar to one positive test except the mean values of r_e are larger.

Several interesting patterns emerge for three positive ice phase tests. First, the overall magnitude of r_e is much larger than with one or two positive tests. Second, zonally symmetric bands emerge with larger values

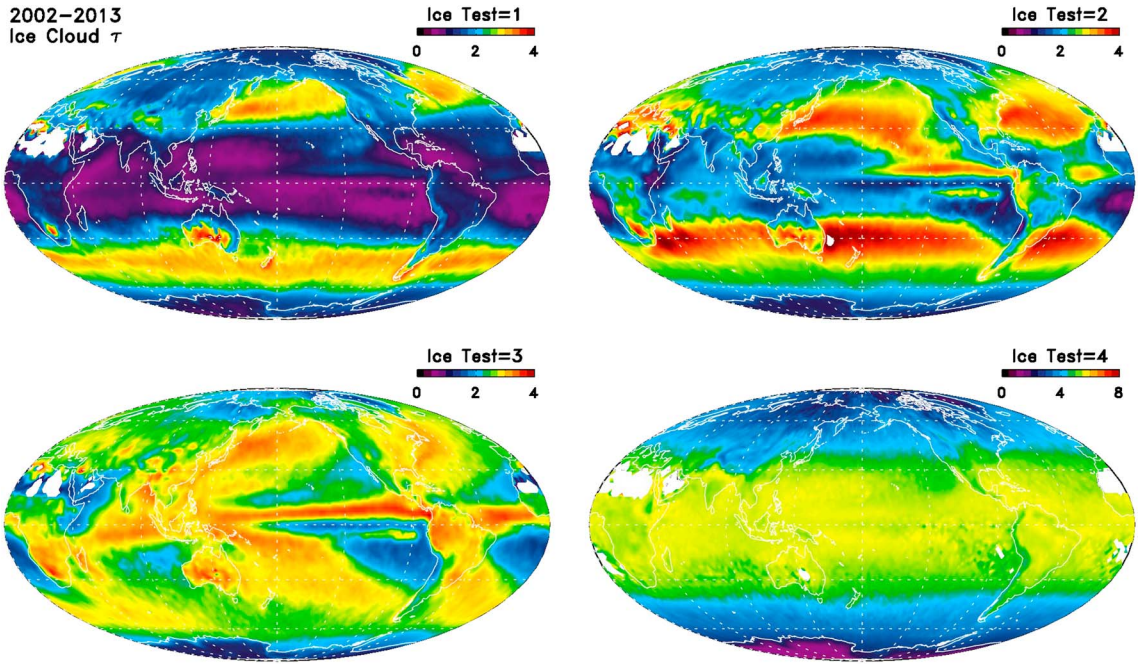

Figure 4. Mean ice cloud τ restricted to the total number of positive AIRS cloud thermodynamic ice phase tests shown in Figure 3. All of the color scales are identical except for four ice phase tests in the bottom right, which is stretched by a factor of 2.

of r_e coinciding with convective regions such as the Intertropical Convergence Zone (ITCZ) and the warm sector portions of midlatitude cyclones that traverse the storm tracks [*Naud and Kahn*, 2015]. Third, very sharp reductions in r_e occur in the midlatitudes, particularly the lee of the Rockies, the Andes, Tasmania, and the south island of New Zealand. These reductions are caused by relatively high proportions of orographic ice clouds that form in strongly ascending regions of standing orographic lee waves. Orographic ice clouds are known to contain very small ice particles and have been previously described in AIRS radiance spectra

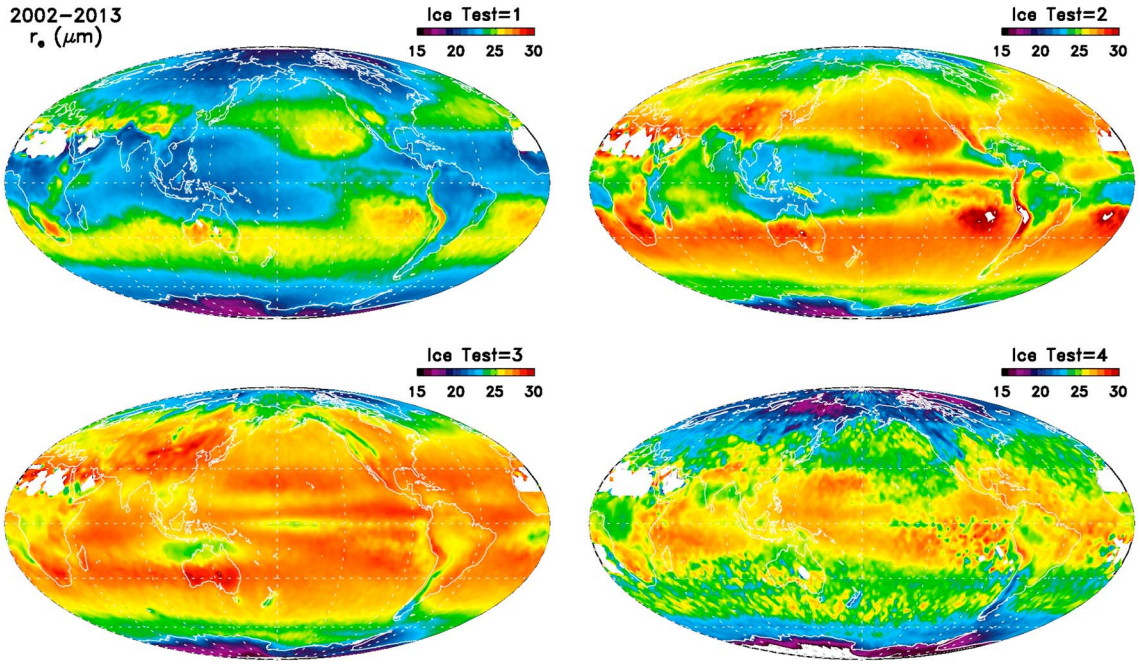

Figure 5. Mean ice cloud r_e restricted to the total number of positive AIRS cloud thermodynamic ice phase tests shown in Figure 3. All of the color scales are identical.

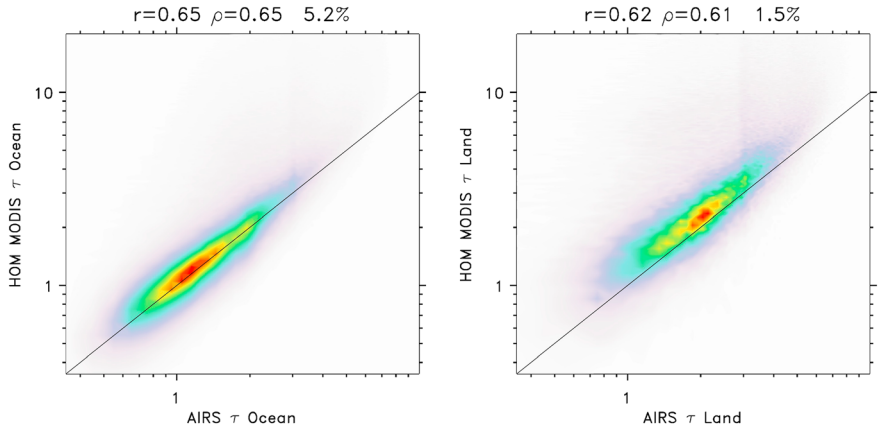

Figure 6. Joint histograms of AIRS and MODIS τ for HOM clouds separated into (left) ocean and (right) land. The Pearson's correlation coefficient (r), Spearman's ranked correlation coefficient (ρ), and the sample size (N) are shown in the title. The one-to-one line is drawn for scale.

[*Kahn et al.*, 2003]. For four positive tests, the values of r_e reach a maximum in the tropics and are reduced toward the poles with somewhat stronger zonal asymmetries compared to τ. This pattern most closely resembles climatological distributions of MODIS r_e [*King et al.*, 2013] albeit with a smaller magnitude.

The vastly different spatial patterns observed in Figures 3–5 strongly depend on the number of positive AIRS ice phase tests and highlight the challenges of using climatological distributions of ice cloud remote sensing retrievals without consideration for the underlying physical processes at work. This suggests that process-based comparisons [e.g., *Naud and Kahn*, 2015] are promising for reconciling the behavior of ice cloud microphysics in observations and climate modeling experiments.

4. Comparisons of τ and r_e Stratified by Scene Complexity

4.1. Land Versus Ocean

Figure 6 compares MODIS and AIRS optical depth retrievals over land and ocean for HOM. The ocean sample size N is more than 3 times larger than land, and slightly higher values of the Pearson's correlation coefficient r and Spearman's ranked correlation coefficient ρ are observed for oceanic clouds. The average bias over ocean is negligible, while a small bias over land is observed. The variability increases with larger τ but more so over land than ocean. The peak occurrence frequencies occur around $\tau = 0.5$–2.0 over ocean and $\tau = 1.0$–5.0 over land. The overland histograms of AIRS τ shift dramatically with the diurnal cycle [*K14*], but only the daytime results apply in this investigation. Little evidence of the AIRS prior guess $\tau = 3.0$ appears over land in Figure 6 but is more apparent in subsets of these histograms (shown later). The elevated scatter and biases over land highlight ongoing challenges for passive ice cloud remote sensing in the VNIR and MIR bands.

Figure 7 shows separate land and ocean r_e scatterplots for HOM. A majority of 2.1 μm r_e retrievals are greater than AIRS by 5–10 μm in the mean with a large amount of scatter. For 1.6 μm r_e retrievals (not shown), the shift is slightly greater than but very similar to 2.1 μm [*Platnick*, 2000]. For 3.7 μm r_e retrievals, the mean values are more or less similar to AIRS r_e retrievals, while r and ρ are notably higher in value (shown later). The scatter is more pronounced at smaller values of r_e (Figure 7), while the opposite is observed with τ having more pronounced scatter at higher values (Figure 6). This suggests that there are reduced consistencies in AIRS and MODIS r_e retrievals at low values of τ (and vice versa).

Next, the pixel-scale cloud complexity is binned to identify physical causes for the systematic biases and variability between AIRS and MODIS r_e retrievals.

4.2. Horizontal Heterogeneity

Figure 8 shows combined land and ocean comparisons of τ separately for HOM, HET, MIX, and DIFF categorizations. The results for the combined land and ocean HOM (Figure 8) are very similar to ocean-only HOM (Figure 6). While both HET and HOM together contain a small systematic bias, larger scatter in the low range

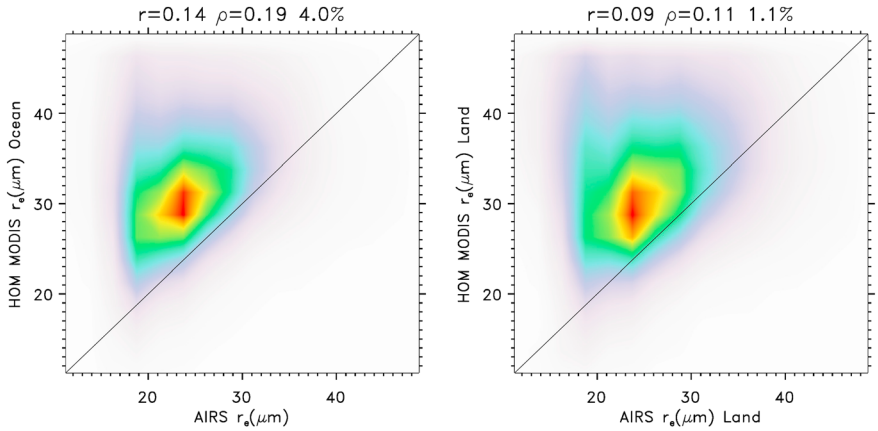

Figure 7. Joint histograms of AIRS and MODIS r_e for HOM clouds separated into (left) ocean and (right) land.

of τ is observed in HET. The total sample size is limited to 1.2% of all available daytime AIRS FOVs; however, this percentage increases to 4.1% or 6.1% if the 1 km or 5 km MIR phase masks, respectively, replace the operational VNIR 1 km phase mask (not shown). Although MIX contains similarly broad scatter as with HET, a larger systematic bias appears at the lower range of τ. In the case of DIFF, AIRS $\tau < 0.5$, while MODIS $\tau = 0.3$–3.0, an even higher bias than in the case of MIX. The larger differences are found in scenes with thin cirrus overlapping low-level liquid cloud [*Davis et al.*, 2009] that is easily detected in the VNIR but not in the MIR. The sample size of DIFF is only 0.8% of all daytime AIRS FOVs. A small percentage is encouraging because this type of cloud configuration has little bearing on the overall cloud climatology.

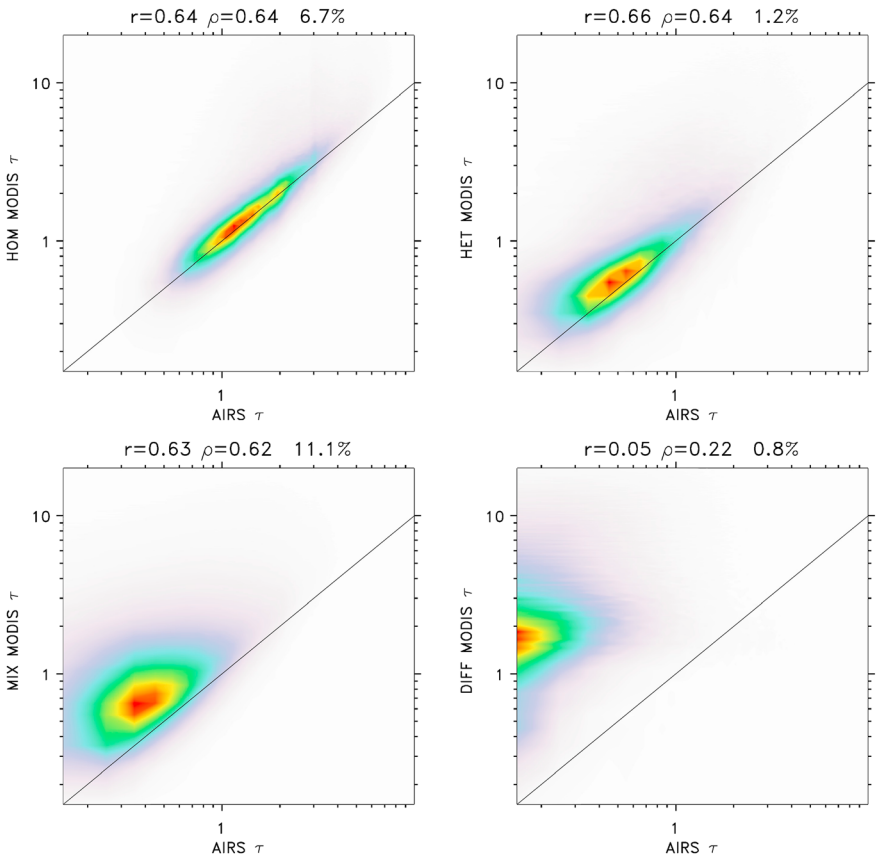

Figure 8. Joint histograms of AIRS and MODIS τ for HOM, HET, MIX, and DIFF clouds for the combined ocean and land.

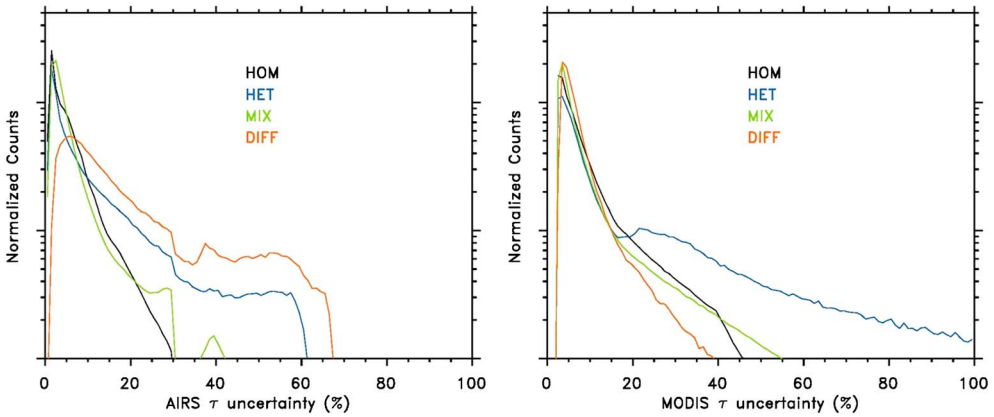

Figure 9. Histograms of AIRS and MODIS τ uncertainties (percent of retrieval value) for HOM, HET, MIX, and DIFF clouds.

The reported AIRS and MODIS τ uncertainties (%) are shown in Figure 9. The uncertainties are lower for HOM and MIX, while they are higher for HET. In AIRS retrievals, the DIFF category has large uncertainties as well that are probably due to overlapping clouds with different thermodynamic phases or subpixel variability. The AIRS AKs (see Appendix A) show reduced values in DIFF cloud scenes, while the χ^2 fitting (see Appendix A) is high for HET cloud scenes. In short, higher uncertainties are associated with complex cloud configurations not accounted for in the single-layer cloud assumption found in the AIRS and MODIS cloud retrievals.

Figure 10 shows comparisons of r_e for HOM, HET, MIX, and DIFF for both 2.1 μm (colors) and 3.7 μm (gray contours) MODIS retrievals. The sample size of HOM is reduced compared to τ (Figure 6) because of the application of the AIRS QC. For the 1.0% of FOVs that are classified as HET, a severe bias arises that is likely caused in part by excessively large values of MODIS r_e along cloud edges [*Platnick et al.*, 2014] that are not identified as partly cloudy. The bias is reduced in MIX cases, but a large amount of scatter remains. This suggests that some MODIS-identified phase mixtures remain at cloud edges and MODIS-derived r_e is biased high in these portions of ice clouds. For DIFF (0.5% of cases), while the bias is negligible, it is encouraging that a poor correlation is observed when there is an obvious disagreement in the AIRS and MODIS thermodynamic phases.

The reported AIRS and MODIS r_e uncertainties are shown in Figure 11. The lowest MODIS 2.1 μm uncertainties are reported in HOM clouds, while AIRS shows similarly low uncertainties for MIX clouds. Slightly elevated uncertainties are found for DIFF in AIRS, while the largest values are found in HET and DIFF clouds for MODIS 2.1 μm retrievals. Interestingly, the uncertainties for MODIS 3.7 μm retrievals are generally larger but the ordering is different than 2.1 μm retrievals. In the case of MODIS 3.7 μm retrievals, the spread of uncertainty caused by horizontal cloud heterogeneity is larger than AIRS unlike τ. This is an indication that AIRS r_e uncertainties [*K14*] are very likely underestimated in the current V6 retrieval, which does not consider ice crystal size and habit distribution uncertainties that can exceed 50% of the value of r_e [e.g., *Posselt et al.*, 2008] but might be improved in a simultaneous VNIR and MIR retrieval [*Baran and Francis*, 2004].

4.3. AIRS Cloud Thermodynamic Phase Tests

To gain further insight on the HOM histograms, Figure 12 shows separate comparisons of τ for one, two, three, and four positive ice phase tests. For one positive test, a highly correlated yet systematic difference is observed between AIRS and MODIS. MODIS is 2–3 times larger when AIRS $\tau > 0.5$. The prior AIRS retrieval guess of $\tau = 3.0$ is clearly seen in the data. For two positive tests, the difference is close to zero for $\tau < 1.0$ with most samples occurring near $\tau = 0.5$–0.7. A small sample of retrievals spreads to larger values of τ. This subpopulation of data is similar to that observed for one positive test. Three positive tests have the largest sample size (3.7%), show very little systematic bias, and have high correlations. Lastly, for four positive tests, approximately 0.6% of AIRS retrievals have values of $\tau = 4$–7 with MODIS scattered substantially higher than AIRS. This is the well-known optical depth saturation limit found in MIR retrievals [e.g., *Huang et al.*, 2004] and highlights the larger dynamic range of sensitivity obtained within VNIR retrievals [*Nakajima and King*, 1990]. This observational capability is especially important for ice phase clouds that occur in deep convection and midlatitude cyclones.

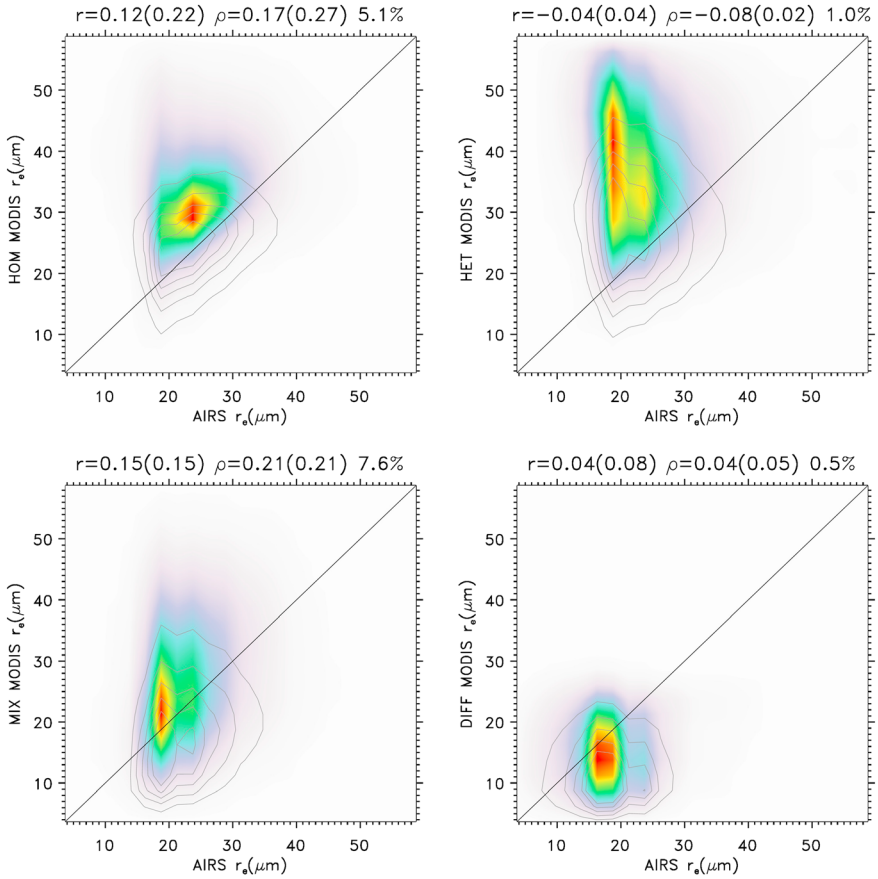

Figure 10. Joint histograms of AIRS and MODIS r_e for HOM, HET, MIX, and DIFF clouds for the combined ocean and land. The colors (gray contours) are for the MODIS 2.1 μm (3.7 μm) band retrievals.

The reported AIRS and MODIS uncertainties are shown in Figure 13. Interestingly, the relative change in uncertainties for both AIRS and MODIS τ tracks the numbers of AIRS ice phase tests, namely, the larger (smaller) the number of tests the smaller (larger) the uncertainty. The AIRS AKs clearly show increased information content for the larger numbers of positive phase tests (see Appendix A). The χ^2 fitting is slightly elevated for three or four phase tests compared to one or two phase tests (see Appendix A) and may reflect more multilayered cloud that occurs with more positive ice phase tests.

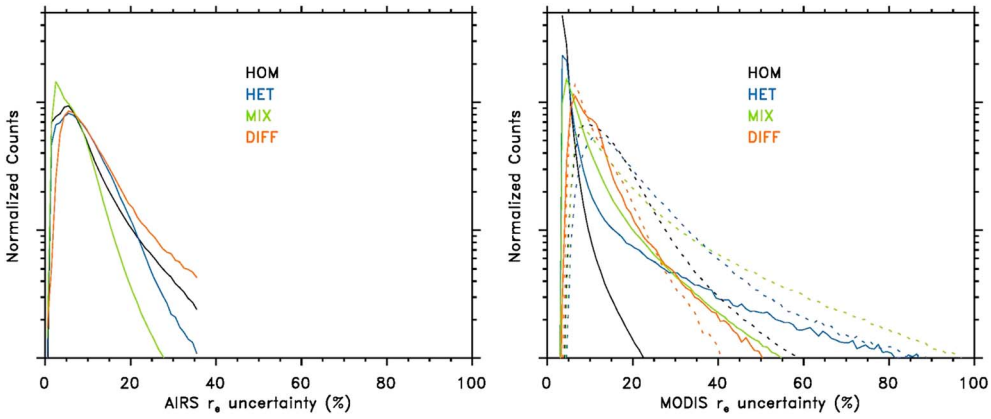

Figure 11. Histograms of AIRS and MODIS r_e uncertainties (percent of retrieval value) for HOM, HET, MIX, and DIFF clouds. The solid (dashed) lines are for the MODIS 2.1 μm (3.7 μm) band retrievals.

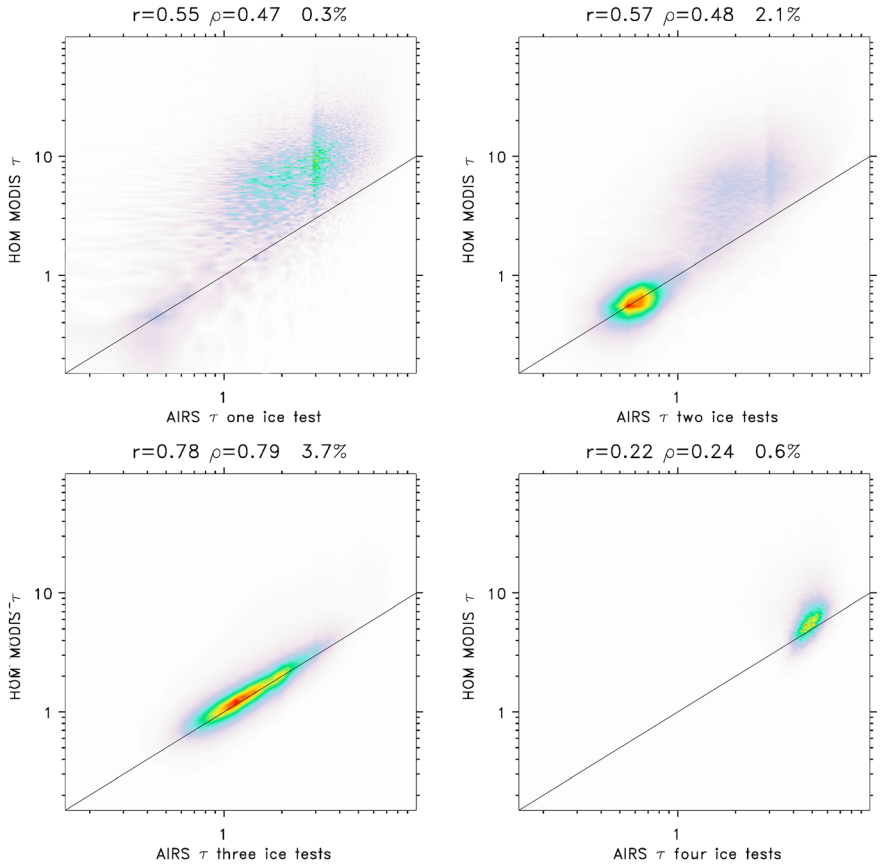

Figure 12. Joint histograms of AIRS and MODIS τ restricted from one to four positive phase tests using the AIRS cloud thermodynamic phase retrieval.

Figure 14 shows separate comparisons of r_e for one to four positive ice phase tests. For one or two positive tests, the scatter in r_e remains very large with MODIS greater than AIRS. For three or four positive tests, both r and ρ are larger than found in one or two positive tests, with a systematic difference of approximately 5 μm observed in the 2.1 μm retrieval and a smaller bias in the 3.7 μm retrieval. While the systematic bias is explained by fundamental radiative transfer differences in MIR and VNIR passive remote sensing [*Zhang et al.*, 2010], the scatter around the mean bias is explained by other factors. *Wang* [2013, cf. Figures 4.27 and 4.28] showed that for the MIR, the spread in the scatter is mainly controlled by uncertainty in (1) the

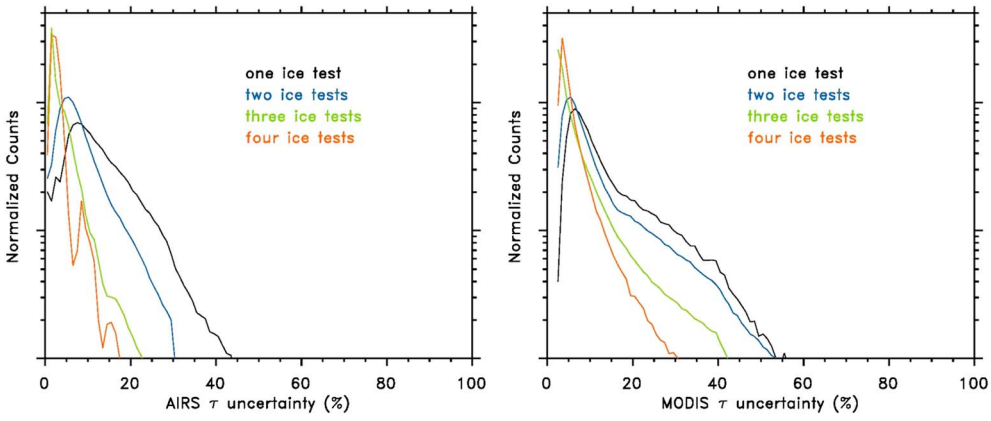

Figure 13. Histograms of AIRS and MODIS τ uncertainties (percent of retrieval value) for one to four positive phase tests as in Figure 12.

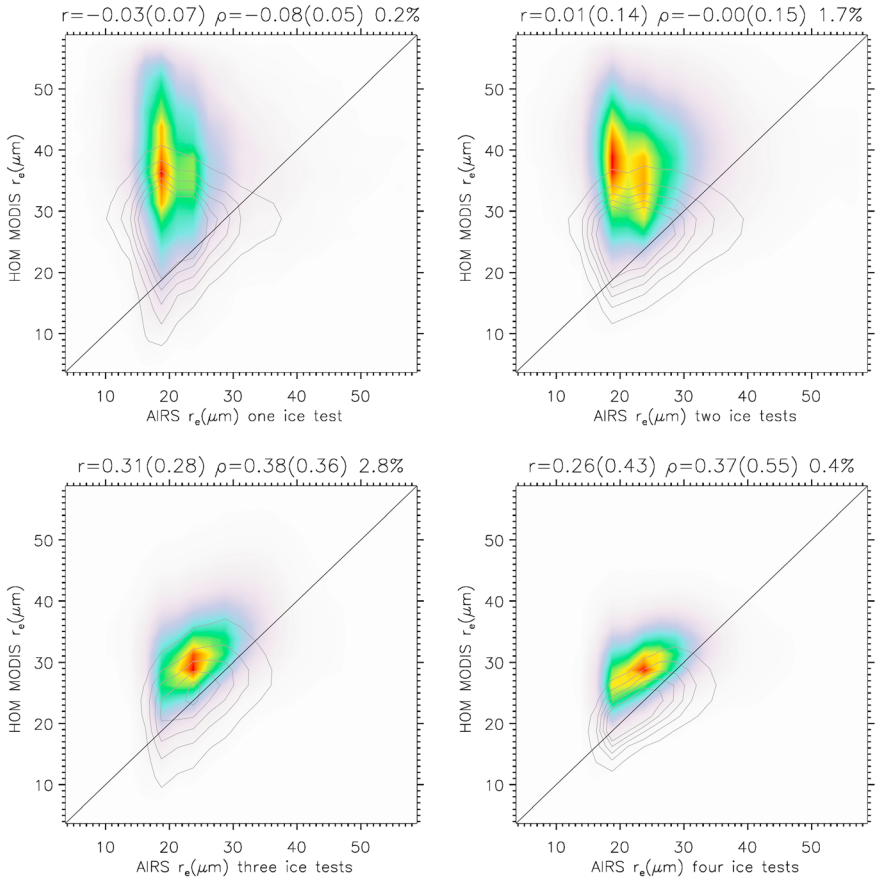

Figure 14. Joint histograms of AIRS and MODIS r_e restricted from one to four positive phase tests using the AIRS cloud thermodynamic phase retrieval. The colors (gray contours) are for the MODIS 2.1 μm (3.7 μm) band retrievals.

width of the ice crystal size distribution, (2) the choice of ice crystal habit mixtures, and (3) the ice crystal surface roughness.

The reported AIRS and MODIS uncertainties are shown in Figure 15. As with τ, the relative ordering of the AIRS r_e uncertainties tracks the number of ice phase tests with less spread in the histograms than τ. A total of four ice phase tests yields especially low uncertainties for both MODIS and AIRS. The MODIS 3.7 μm uncertainties have magnitudes more similar to AIRS than the 2.1 μm retrievals and suggest that the 2.1 μm r_e uncertainties may be underestimated.

4.4. Single-Layered Versus Multilayered Clouds

Table 3 summarizes comparisons of τ binned by multilayered cloud metrics. When either multilayer metric is used to filter clouds, the values of r and ρ are found to increase since clouds are restricted to single-layered HOM FOVs. However, N is reduced for both metrics and is further reduced with increasingly stringent criteria for single-layered clouds (not shown). When both multilayer metrics are applied simultaneously, the values of r and ρ (1.3% of all cases) reach the highest correlations (0.95 and 0.92, respectively) of any data subset investigated in this work. We conclude that multilayered clouds are a significant source of the scatter in τ that is caused by the assumption of a single-layer cloud in either the VNIR or the MIR retrieval, similar to previous studies [*Niu et al.*, 2007; *Ham et al.*, 2009; *Ham and Sohn*, 2012]. Similar conclusions are also reached for the 2.1 and 3.7 μm r_e comparisons (Table 4) with the largest values of r and ρ occurring when both metrics are applied simultaneously. However, a bias of 5–10 μm remains between AIRS and MODIS retrievals [*Zhang et al.*, 2010].

4.5. Latitude Dependence

Figure 16 shows comparisons of oceanic τ that are stratified by zonal bands. The occurrence frequencies for all panels in Figure 16 sum to the occurrence frequency reported for oceanic HOM in Figure 6. Correlations of

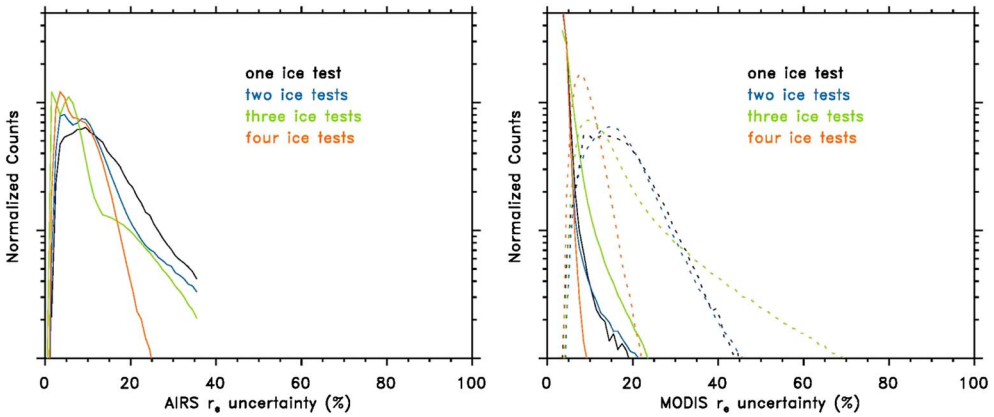

Figure 15. Histograms of AIRS and MODIS r_e uncertainties (percent of retrieval value) for one to four positive phase tests as in Figure 14. Note that the MODIS 3.7 μm retrievals agree much more closely with AIRS in magnitude and relative ordering of the histograms.

$r = 0.81$ and $\rho = 0.88$ are found in the tropical latitudes (±20°) and are somewhat reduced in the subtropical latitudes (±20–40°N/S). There are two climatological factors at play that may explain this behavior. First, according to in situ observations, tropical ice clouds are more vertically homogeneous than found at other latitudes [e.g., *Heymsfield et al*., 2006; *Liou et al*., 2008]. Second, although the rate of occurrence of multilayered ice clouds is highest in the tropics and within the midlatitude storm tracks, the multilayer clouds in the tropics are almost exclusively high cirrus clouds overlapping shallow trade cumulus clouds [*Chang and Li*, 2005; *Mace et al*., 2009]. Since trade cumulus clouds are broken and contain small cloud fractions and thus contribute marginally to the overall signal of the MODIS VNIR reflectance functions, the expectation is that the VNIR and MIR retrievals will be most consistent for tropical cirrus. In the midlatitudes, the most common multilayer cloud is overlapping high-level and middle-level clouds [*Mace et al*., 2009]. The midlevel clouds have high cloud fractions and are optically thick. As a result, these midlevel clouds will contribute more strongly to the VNIR reflectance functions and reduced MIR thermal contrast, leading to larger discrepancies in both τ and r_e retrievals.

In the polar latitudes (±60–90°N/S), the scatter between AIRS and MODIS is very broad. Interestingly, there is a very small bias in τ that flips sign from the tropics where MODIS is slightly larger than AIRS to the midlatitudes where AIRS is slightly larger than MODIS. The latitudinal dependence is similar to the dependence observed with solar zenith angle (θ_s) (not shown). For low values of θ_s, which preferentially are located in the tropics, MODIS $\tau >$ AIRS τ. The opposite is true for $\theta_s > 50$–60° that occurs at high latitudes and also at the edges of the instrument swaths in the lower latitudes. The potential causes of the very small latitudinal and θ_s dependence in the bias are not currently known. However, we point out that initial comparisons with MODIS collection 5 τ and r_e showed much larger θ_s biases and may be related to the assumed ice cloud scattering models used.

The uncertainties in AIRS and MODIS τ are shown in Figure 17. The lowest uncertainties for both AIRS and MODIS are in the tropical and subtropical latitudes with the largest values found in polar latitudes. The AIRS AKs (Appendix A) track the uncertainty while χ^2 does not, suggesting that the large AIRS uncertainties in polar regions are due to reduced information content. A reduction in information content in higher latitudes is expected in part due to reduced thermal contrast between the ice cloud and surface temperatures

Table 3. Pearson's Correlation Coefficient (r), Spearman's Ranked Correlation Coefficient (ρ), and the Percentage of Sample Size N for AIRS and MODIS τ Comparisons in Single-Layer and Multilayered Cloud Configurations

MODIS τ	AIRS τ	r	ρ	N
HOM	All	0.64	0.64	6.7%
HOM	Lower layer ECF < 0.1	0.78	0.86	3.0%
Multilayer < 1.5 HOM	All	0.86	0.86	2.3%
Multilayer < 1.5 HOM	Lower layer ECF < 0.1	0.95	0.92	1.3%

Table 4. Values of r, ρ, and N for AIRS and MODIS r_e Comparisons Within Single-Layer and Multilayered Cloud Configurations[a]

MODIS r_e	AIRS r_e	r	ρ	N
HOM 2.1 μm	All	0.12	0.17	5.1%
HOM 3.7 μm	All	0.22	0.27	5.1%
HOM 2.1 μm	Lower layer ECF < 0.1	0.24	0.32	2.2%
HOM 3.7 μm	Lower layer ECF < 0.1	0.26	0.34	2.2%
Multilayer < 1.5 HOM 2.1 μm	All	0.25	0.33	1.8%
Multilayer < 1.5 HOM 3.7 μm	All	0.27	0.35	1.8%
Multilayer < 1.5 HOM 2.1 μm	Lower layer ECF < 0.1	0.39	0.42	1.0%
Multilayer < 1.5 HOM 3.7 μm	Lower layer ECF < 0.1	0.31	0.38	1.0%

[a]Values for both the 2.1 μm and 3.7 μm MODIS retrievals are shown.

and increased frequency of deep tropospheric isothermal layers and surface-based inversions. Similar results for r_e are shown in Table 5 and are largely consistent with the previous discussion, namely, the highest (lowest) correlations are found in the low (high) latitudes.

4.6. Other Factors

The MODIS cloud top temperature (T_{cld}) product is used to further stratify the r_e and τ comparisons. The strongest correlations are found for the colder cloud tops ($T_{cld} < 235$ K), with poorer correlations for $T_{cld} > 250$ K. The MODIS radiance variance for channel 31 shows some indication that, paradoxically, better agreement is found in more variable scenes. However, this behavior is convoluted with the T_{cld} dependence and further depends on cloud type and it is challenging to discern a meaningful dependence on small-scale radiance

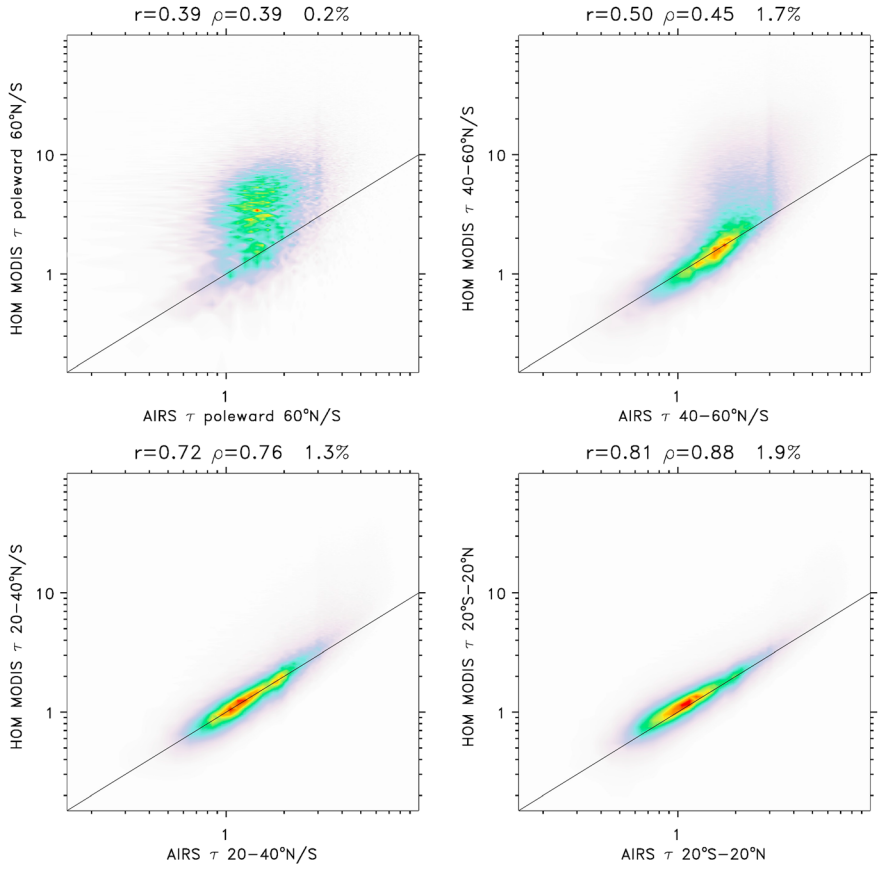

Figure 16. Joint histograms of AIRS and MODIS τ restricted to four latitudinal bands in the polar regions, midlatitudes, subtropics, and tropics (clockwise, from top left).

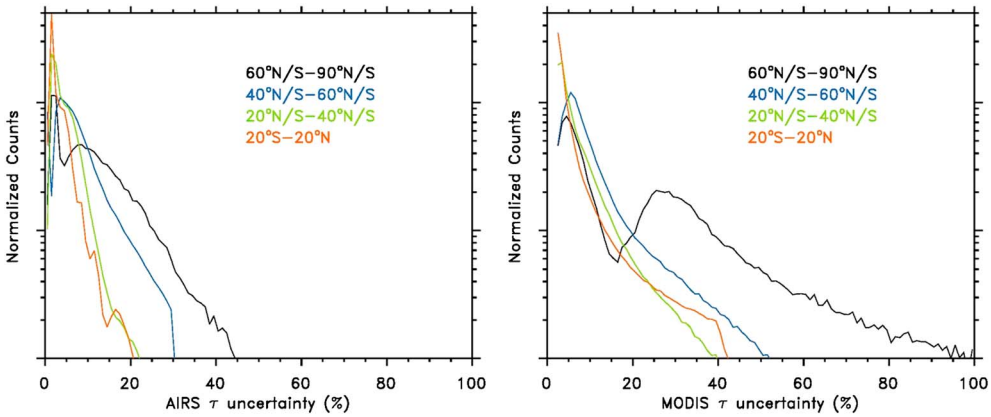

Figure 17. Histograms of AIRS and MODIS τ uncertainties (percent of retrieval value) for the four latitudinal bands shown in Figure 16.

variability without extensive further research. Despite this, the results presented herein suggest that horizontal heterogeneity should play a larger role in future AIRS retrieval modifications.

The τ uncertainty estimates are more consistent between AIRS and MODIS than the r_e uncertainty estimates. The cloud thermodynamic phase uncertainty should also be quantitatively accounted for as evidenced by the dependence on the number of positive AIRS ice phase tests, which could serve as a proxy for phase uncertainty.

The vertical inhomogeneity and multilayering of clouds is also a primary source of reduced agreement in r_e and τ comparisons. Furthermore, the scatter in r_e comparisons may be considered as additional unexploited information contained in the vertical profile that could be retrieved in a simultaneous AIRS and MODIS retrieval. Current research is focused on using active CloudSat radar and CALIPSO lidar profiles as further constraints on the vertical distribution of hydrometeors [e.g., *Delanoë and Hogan*, 2010].

5. Discussion and Summary

Passive satellite remote sensing retrievals of ice cloud optical and microphysical properties remain poorly characterized and are underutilized in climate model validation efforts. To understand the ice cloud property retrievals as a function of cloud complexity at the native sensor resolution, we describe pixel-scale comparisons of collocated AIRS and MODIS ice cloud optical thickness (τ) and effective radius (r_e). The comparisons are partitioned by horizontal variability in cloud fraction and cloud top thermodynamic phase, the presence of single-layer or multilayer clouds, the underlying surface, latitude, and additional geophysical parameters of interest. The pixel-scale uncertainty estimates that are reported along with the AIRS version 6 and MODIS collection 6 retrievals of τ and r_e are shown and compared for a wide variety of pixel-scale cloud complexity.

More than half of the ice-containing AIRS FOVs (26.5% of all AIRS FOVs) have at least some ice according to the MODIS VNIR phase mask. The remaining AIRS FOVs that detect ice are almost always clear according to

Table 5. Latitude Sorting of Values of r, ρ, and N for AIRS and MODIS r_e Comparisons[a]

MODIS/AIRS r_e	Latitude	r	ρ	N
HOM 2.1 μm	20°S–20°N	0.35	0.45	1.6%
HOM 3.7 μm	20°S–20°N	0.29	0.41	1.6%
HOM 2.1 μm	20–40°N/S	0.24	0.29	1.3%
HOM 3.7 μm	20–40°N/S	0.29	0.35	1.3%
HOM 2.1 μm	40–60°N/S	0.02	0.03	1.8%
HOM 3.7 μm	40–60°N/S	0.11	0.13	1.8%
HOM 2.1 μm	60–90°N/S	0.05	0.09	0.4%
HOM 3.7 μm	60–90°N/S	0.07	0.05	0.4%

[a]Values for both the 2.1 μm and 3.7 μm MODIS retrievals are shown.

the MODIS VNIR phase mask. We further stratify the comparisons by horizontal heterogeneity within the AIRS FOV: uniform ice (HOM), broken ice (HET), ice and liquid mixtures (MIX), and liquid only when AIRS reports ice (DIFF) to characterize phase disagreement. HOM and HET FOVs show a higher proportion of valid AIRS r_e retrievals than MIX FOVs. This shows that the AIRS QC approach is appropriately handling the presence of more complex cloud scenes that is reflected in reduced values of scalar averaging kernels (AKs) and poorer χ^2 spectral fits. Furthermore, the reduction of valid r_e retrievals in complex cloud configurations lends confidence to the AIRS operational retrieval approach and suggests that a combined AIRS and MODIS ice cloud retrieval may help characterize some of these complex clouds more correctly.

The frequency of one or two AIRS positive ice phase tests is higher in the midlatitude storm tracks and over land especially near topographic features, while three or four positive tests are reflected in the patterns of subtropical and tropical thin cirrus and deep convection over land. Ice cloud τ tends to increase with more positive ice phase tests especially in the tropical convective regions. In the storm track regions, higher τ is found in the western ocean basins where cyclogenesis is common. For four positive ice phase tests, a zonally symmetric pattern is seen and is spatially very similar to MODIS τ distributions [*King et al*., 2013]. This demonstrates overlapping sensitivity in optically thicker ice clouds.

Smaller values of r_e coincide with low values of τ in tropical thin cirrus. Larger values of r_e are shifted equatorward relative to the maximum value of τ found within the oceanic storm tracks. For three positive tests, the overall magnitude of r_e is higher. Zonally symmetric bands are observed and relate to the positioning of the ITCZ and the storm tracks. Very sharp reductions of r_e are observed in the lee of major topographical features within the midlatitude westerlies and are associated with small ice particles generated within standing orographic lee waves. For four positive tests, values of r_e are at a maximum in the tropics and are reduced toward the poles and resemble MODIS retrievals [*King et al*., 2013], further demonstrating overlapping sensitivity for thicker ice clouds. Also, overall MODIS r_e is a little larger than AIRS and is consistent with the narrowband radiative transfer simulations described in *Zhang et al*. [2010].

No τ bias is observed over ocean, while a small τ bias is observed over land. The r_e biases over land and ocean are quite similar and show significant scatter and a consistent bias of 5–10 μm for the MODIS 2.1 μm band, while the scatter and bias are reduced for the MODIS 3.7 μm band. Much more scatter in AIRS and MODIS r_e is observed in HET scenes compared to HOM scenes. Larger differences in r_e are found in scenes with overlapping clouds compared to single-layer clouds. The reported AIRS and MODIS uncertainty estimates are lower for HOM and MIX, while they are highest for HET.

For the HET FOVs (1.0%), a severe bias in r_e is observed and is possibly caused by large values of MODIS r_e along cloud edges that are not included in the "partly cloudy" designation. The lowest MODIS uncertainties are reported in HOM clouds. Comparisons of the spread of uncertainties in AIRS and MODIS r_e suggest that the AIRS r_e uncertainty estimates are likely underestimated in magnitude and require further development. When τ comparisons are restricted to one positive ice phase test, they show a systematic bias and large scatter; a clear signature of the AIRS prior guess $\tau = 3.0$ is also observed. Two and three positive ice phase tests show a τ bias essentially near zero with little scatter. Four positive tests demonstrate the saturation of the AIRS MIR signal in ice clouds. For r_e, one or two positive tests show large amounts of scatter but it is greatly reduced for three or four tests with a consistent 5 μm bias remaining for the 2.1 μm retrieval [e.g., *Zhang et al*., 2010]. The relative ordering of r_e uncertainty estimates track the number of ice phase tests but are generally lower than reported with τ.

When either the AIRS lower layer effective cloud fraction or the MODIS multilayer flag is used to restrict the comparison to single-layer clouds, the correlations substantially increase. When both multilayer metrics are simultaneously used, the highest correlations are observed among all data subsets investigated. The highest correlations for both r_e and τ within all clouds are found in the tropics where ice clouds are more vertically homogeneous. The polar latitudes show very broad scatter in both r_e and τ. Reassuringly, the lowest uncertainty estimates are found in the tropical and subtropical latitudes and the largest are found in the polar latitudes. A reduction in AIRS information content with increasing latitude is consistent with a reduced thermal contrast between the surface and the ice cloud altitude.

These comparisons show that we must reconcile the pixel-scale variability of clouds in order to unravel the individual strengths of AIRS and MODIS ice cloud property retrievals and to maximize their usefulness as climate data records. This comparison will serve as a useful benchmark for ice cloud observational records obtained

from similar instruments in orbit, specifically the Visible Infrared Imaging Radiometer Suite (VIIRS) and Cross-track Infrared Sounder (CrIS), and ensure climate quality continuity over a multidecadal time period.

Appendix A

To gain further insight regarding the AIRS uncertainties and information content, the AK histograms of τ are shown in Figure A1. The histograms are organized by cloud heterogeneity (HOM, HET, MIX, and DIFF), latitude (tropical, subtropical, midlatitude, and polar), restricted to single-layer clouds, and the number of positive ice

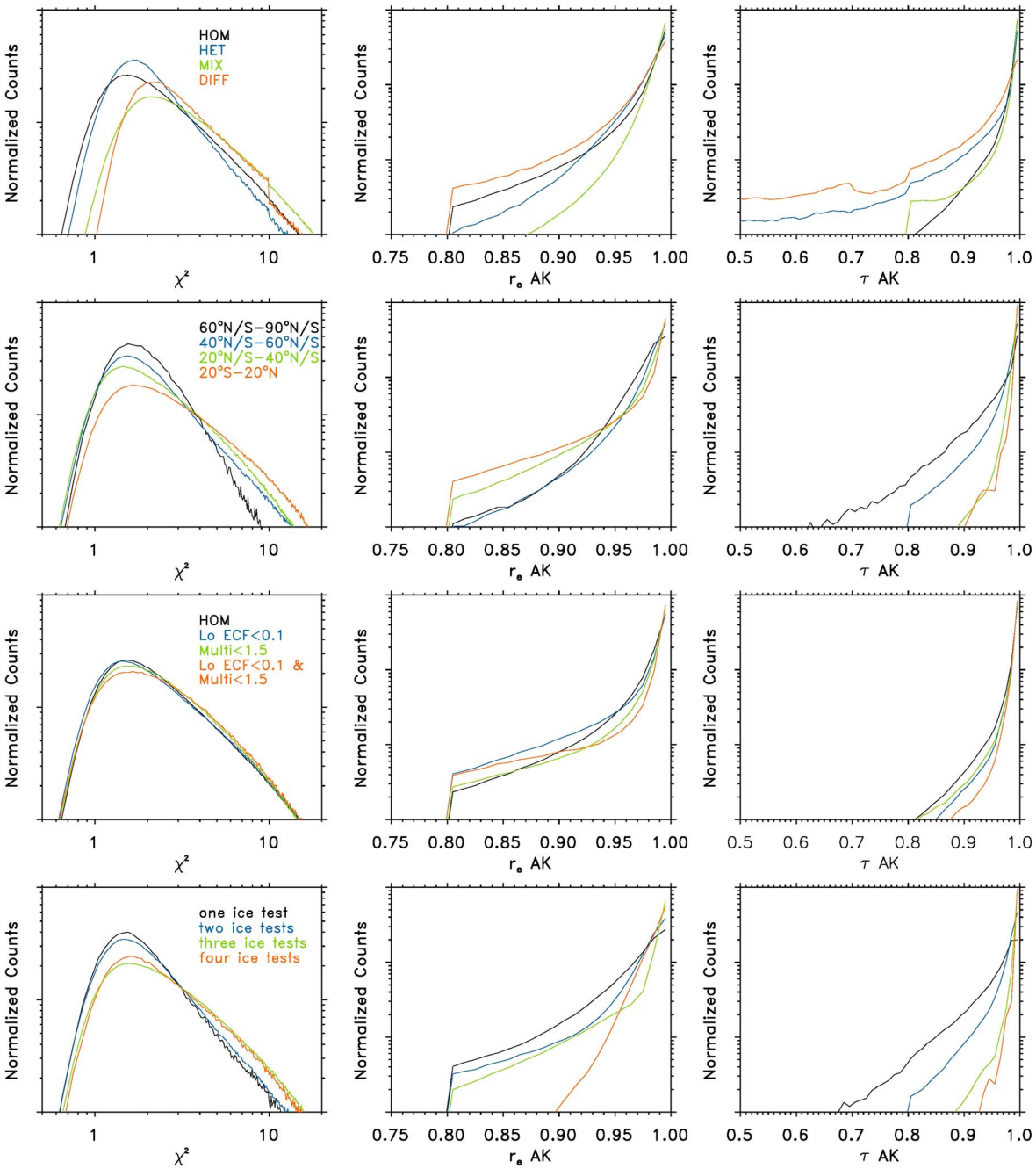

Figure A1. AIRS normalized χ^2 sorted by (left column) cloud heterogeneity, (middle column) AIRS scalar averaging kernels (AKs) for r_e, and (right column) scalar AKs for τ. All histograms are sorted by (first row) cloud heterogeneity, (second row) latitude, (third) single-layer versus multilayer cloud, and (fourth row) the number of positive cloud thermodynamic ice phase tests passed.

phase tests passed (1–4). The HET and DIFF scenes have the largest frequency of occurrence of low values of AKs that is very similar to the retrieval uncertainties. There is a clear relationship with AKs and latitude, in which the highest (lowest) values tend to be found in the lowest (highest) latitudes. There is less impact of multilayer cloud structure on AKs, although slightly higher values are found for the most stringent filtering for single-layer clouds. A very clear relationship is observed between the number of ice phase tests and the AK distributions, with higher values found for a larger number of passing tests.

The AK histograms of r_e are shown in Figure A1. The DIFF (MIX) scenes have the largest (smallest) occurrence frequencies of low values of AKs. This may suggest that MIX scenes might be composed of some uniform thin cirrus and also some phase misclassification in either/both AIRS or MODIS. Unlike τ, the AKs have an opposite dependence on latitude, although this is likely a reflection of the preponderance of optically thin cirrus clouds with reduced information content. There is a small impact of multilayer cloud structure on r_e AKs, with the most stringent filtering for single-layer clouds yielding the highest values of AKs. A less obvious relationship is observed for the number of ice phase tests passed and the r_e AKs, although the highest values are found for four passing tests.

The histograms of χ^2 are shown in Figure A1. Interestingly, the largest variations in the quality of the spectral fits are related to cloud horizontal heterogeneity, with the worst fits in MIX and DIFF FOVs. More surprisingly, very little dependence is found for χ^2 and the filtering for single-layer clouds. The dependence of χ^2 with latitude shows slightly worse fits in the low latitudes, which is unsurprising given the much higher thermal contrast in these latitudes. Also, a weak dependence on the number of ice phase tests is found.

Acknowledgments

A portion of this research was carried out at the Jet Propulsion Laboratory (JPL), California Institute of Technology, under a contract with the National Aeronautics and Space Administration. The AIRS version 6 and MODIS collection 6 data sets were processed by and obtained from the Goddard Earth Services Data and Information Services Center (http://daac.gsfc.nasa.gov/) and the Level 1 and Atmosphere and Archive Distribution System (http://ladsweb.nascom.nasa.gov). B.H.K. was supported by the NASA Science of Terra and Aqua program under grant NNN13D455T and the AIRS Project at JPL. The authors thank the three anonymous reviewers for their constructive comments and Donifan Barahona, Andrew Gettelman, and Lazaros Oreopoulos for the conversations that helped benefit the focus of this work.

References

Ackerman, S. A., R. E. Holz, R. Frey, E. W. Eloranta, B. C. Maddux, and M. McGill (2008), Cloud detection with MODIS. Part II: Validation, *J. Atmos. Oceanic Technol.*, *25*, 1073–1086.

Barahona, D., J. Rodriguez, and A. Nenes (2010), Sensitivity of the global distribution of cirrus ice crystal concentration to heterogeneous freezing, *J. Geophys. Res.*, *115*, D23213, doi:10.1029/2010JD014273.

Baran, A. J., and P. N. Francis (2004), On the radiative properties of cirrus cloud at solar and thermal wavelengths: A test of model consistency using high-resolution airborne radiance measurements, *Q. J. R. Meteorol. Soc.*, *130*, 763–778.

Baum, B. A., W. P. Menzel, R. A. Frey, D. C. Tobin, R. E. Holz, S. A. Ackerman, A. K. Heidinger, and P. Yang (2012), MODIS cloud-top property refinements for collection 6, *J. Appl. Meteorol. Climatol.*, *51*, 1145–1163, doi:10.1175/JAMC-D-11-0203.1.

Cesana, G., J. E. Kay, H. Chepfer, J. M. English, and G. de Boer (2012), Ubiquitous low-level liquid-containing Arctic clouds: New observations and climate model constraints from CALIPSO-GOCCP, *Geophys. Res. Lett.*, *39*, L20804, doi:10.1029/2012GL053385.

Chang, F.-L., and Z. Li (2005), A near-global climatology of single-layer and overlapped clouds and their optical properties retrieved from Terra/MODIS data using a new algorithm, *J. Clim.*, *18*, 4752–4771.

Cheng, A., K.-M. Xu, Y. Hu, and S. Kato (2012), Impact of a cloud thermodynamic phase parameterization based on CALIPSO observations on climate simulation, *J. Geophys. Res.*, *117*, D09103, doi:10.1029/2011JD017263.

Cho, H.-M., S. L. Nasiri, and P. Yang (2009), Application of CALIOP measurements to the evaluation of cloud phase derived from MODIS infrared channels, *J. Appl. Meteorol. Climatol.*, *48*, 2169–2180, doi:10.1175/2009JAMC2238.1.

Chung, S., S. Ackerman, P. F. van Delst, and W. P. Menzel (2000), Model calculations and interferometer measurements of ice-cloud characteristics, *J. Appl. Meteorol.*, *39*, 634–644.

Cooper, S. J., T. S. L'Ecuyer, and G. L. Stephens (2003), The impact of explicit cloud boundary information on ice cloud microphysical property retrievals from infrared radiances, *J. Geophys. Res.*, *108*(D3), 4107, doi:10.1029/2002JD002611.

Cooper, S. J., T. S. L'Ecuyer, P. Gabriel, A. J. Baran, and G. L. Stephens (2006), Objective assessment of the information content of visible and infrared radiance measurements for cloud microphysical property retrievals over the global oceans. Part II: Ice clouds, *J. Appl. Meteorol. Climatol.*, *45*, 42–62.

Cooper, S. J., T. S. L'Ecuyer, P. Gabriel, A. J. Baran, and G. L. Stephens (2007), Performance assessment of a five-channel estimation-based ice cloud retrieval scheme for use over the global oceans, *J. Geophys. Res.*, *112*, D04207, doi:10.1029/2006JD007122.

Davis, S. M., L. M. Avallone, B. H. Kahn, K. G. Meyer, and D. Baumgardner (2009), Comparison of airborne in situ measurements and Moderate Resolution Imaging Spectroradiometer (MODIS) retrievals of cirrus cloud optical and microphysical properties during the Midlatitude Cirrus Experiment (MidCiX), *J. Geophys. Res.*, *114*, D02203, doi:10.1029/2008JD010284.

Delanoë, J., and R. J. Hogan (2008), A variational scheme for retrieving ice cloud properties from combined radar, lidar, and infrared radiometer, *J. Geophys. Res.*, *113*, D07204, doi:10.1029/2007JD009000.

Delanoë, J., and R. J. Hogan (2010), Combined CloudSat-CALIPSO-MODIS retrievals of the properties of ice clouds, *J. Geophys. Res.*, *115*, D00H29, doi:10.1029/2009JD012346.

Deng, M., G. G. Mace, Z. Wang, and R. P. Lawson (2013), Evaluation of several A-Train ice cloud retrieval products with in situ measurements collected during the SPARTICUS campaign, *J. Appl. Meteorol. Climatol.*, *52*, 1014–1030.

European Space Agency (ESA) (2004), EarthCARE—Earth Clouds, Aerosols and Radiation Explorer Technical and Programmatic Annex, Reports for Mission Selection–The Six Candidate Earth Explorer Missions, 47 pp. [Available at http://www.esa.int/Our_Activities/Observing_the_Earth/The_Living_Planet_Programme/Earth_Explorers/EarthCARE/ESA_s_cloud_aerosol_and_radiation_mission.]

Frey, R. A., S. A. Ackerman, Y. Liu, K. I. Strabala, H. Zhang, J. R. Key, and X. Wang (2008), Cloud detection with MODIS. Part I: Improvements in the MODIS cloud mask for collection 5, *J. Atmos. Oceanic Technol.*, *25*, 1057–1072, doi:10.1175/2008JTECHA1052.1.

Gettelman, A., X. Liu, S. J. Ghan, H. Morrison, S. Park, A. J. Conley, S. A. Klein, J. Boyle, D. L. Mitchell, and J.-L. F. Li (2010), Global simulations of ice nucleation and ice supersaturation with an improved cloud scheme in the Community Atmosphere Model, *J. Geophys. Res.*, *115*, D18216, doi:10.1029/2009JD013797.

Guignard, A., C. J. Stubenrauch, A. J. Baran, and R. Armante (2012), Bulk microphysical properties of semi-transparent cirrus from AIRS: A six year global climatology and statistical analysis in synergy with geometrical profiling data from CloudSat-CALIPSO, *Atmos. Chem. Phys.*, *12*, 503–525.

Ham, S.-H., and B.-J. Sohn (2012), Vertical-homogeneity assumption causing inconsistency between visible- and infrared-based cloud optical properties, *IEEE Geosci. Remote Sens. Lett.*, *9*, 531–535.

Ham, S.-H., B.-J. Sohn, P. Yang, and B. A. Baum (2009), Assessment of the quality of MODIS cloud products from radiance simulations, *J. Appl. Meteorol. Climatol.*, *48*, 1591–1612.

Hendricks, J., B. Kärcher, and U. Lohmann (2011), Effects of ice nuclei on cirrus clouds in a global climate model, *J. Geophys. Res.*, *116*, D18206, doi:10.1029/2010JD015302.

Heymsfield, A. J., C. Schmitt, A. Bansmer, G.-J. van Zadelhoff, M. J. McGill, C. Twohy, and D. Baumgardner (2006), Effective radius of ice cloud particle populations derived from aircraft probes, *J. Atmos. Oceanic Technol.*, *23*, 361–380.

Hoskins, B. J., and K. I. Hodges (2002), New perspectives on the Northern Hemisphere winter storm tracks, *J. Atmos. Sci.*, *59*, 1041–1061.

Hu, Y., et al. (2009), CALIPSO/CALIOP cloud phase discrimination algorithm, *J. Atmos. Oceanic Technol.*, *26*, 2293–2309.

Huang, H.-L., P. Yang, H. Wei, B. A. Baum, Y. Hu, P. Antonelli, and S. A. Ackerman (2004), Inference of ice cloud properties from high spectral resolution infrared observations, *IEEE Trans. Geosci. Remote Sens.*, *42*, 842–853.

IPCC (2013), *Climate Change 2013: The Physical Science Basis. Contribution of Working Group I to the Fifth Assessment Report of the Intergovernmental Panel on Climate Change*, edited by T. F. Stocker, et al., 1535 pp., Cambridge Univ. Press, Cambridge, U. K., and New York, doi:10.1017/CBO9781107415324.

Jin, H., and S. L. Nasiri (2014), Evaluation of AIRS cloud-thermodynamic-phase determination with CALIPSO, *J. Appl. Meteorol. Climatol.*, *53*, 1012–1026.

Kahn, B. H., A. Eldering, S. A. Clough, E. J. Fetzer, E. F. Fishbein, M. R. Gunson, S.-Y. Lee, P. F. Lester, and V. J. Realmuto (2003), Near micron-sized cirrus cloud particles in high-resolution infrared spectra: An orographic case study, *Geophys. Res. Lett.*, *30*(8), 1441, doi:10.1029/2003GL016909.

Kahn, B. H., C. K. Liang, A. Eldering, A. Gettelman, Q. Yue, and K. N. Liou (2008), Tropical thin cirrus and relative humidity observed by the Atmospheric Infrared Sounder, *Atmos. Chem. Phys.*, *8*, 1501–1518.

Kahn, B. H., S. L. Nasiri, M. M. Schreier, and B. A. Baum (2011), Impacts of sub-pixel cloud heterogeneity on infrared thermodynamic phase assessment, *J. Geophys. Res.*, *116*, D20201, doi:10.1029/2011JD015774.

Kahn, B. H., et al. (2014), The Atmospheric Infrared Sounder version 6 cloud products, *Atmos. Chem. Phys.*, *14*, 399–426.

King, M. D., S. Platnick, W. P. Menzel, S. A. Ackerman, and P. A. Hubanks (2013), Spatial and temporal distributions of clouds observed by MODIS onboard the Terra and Aqua satellites, *IEEE Trans. Geosci. Remote Sens.*, *51*, 3826–3852.

Liou, K. N. (1986), Influence of cirrus clouds on weather and climate processes: A global perspective, *Mon. Weather Rev.*, *114*, 1167–1199.

Liou, K. N., Y. Gu, Q. Yue, and G. McFarquhar (2008), On the correlation between ice water content and ice crystal size and its application to radiative transfer and general circulation models, *Geophys. Res. Lett.*, *35*, L13805, doi:10.1029/2008GL033918.

Lohmann, U., and B. Karcher (2002), First interactive simulations of cirrus clouds formed by homogeneous freezing in the ECHAM general circulation model, *J. Geophys. Res.*, *107*(D10), 4105, doi:10.1029/2001JD000767.

Mace, G. G., Q. Zhang, M. Vaughan, R. Marchand, G. Stephens, C. Trepte, and D. Winker (2009), A description of hydrometeor layer occurrence statistics derived from the first year of merged CloudSat and CALIPSO data, *J. Geophys. Res.*, *114*, D00A26, doi:10.1029/2007JD009755.

Menzel, W. P., R. A. Frey, H. Zhang, D. P. Wylie, C. C. Moeller, R. E. Holz, B. Maddux, B. A. Baum, K. I. Strabala, and L. E. Gumley (2008), MODIS global cloud-top pressure and amount estimation: Algorithm description and results, *J. Appl. Meteorol. Climatol.*, *47*, 1175–1198.

Miller, S. D., G. L. Stephens, C. K. Drummond, A. K. Heidinger, and P. T. Partain (2000), A multisensory diagnostic satellite cloud property retrieval scheme, *J. Geophys. Res.*, *105*, 19,955–19,971.

Mitchell, D. L., P. Rasch, D. Ivanova, G. McFarquhar, and T. Nousiainen (2008), Impact of small ice crystal assumptions on ice sedimentation rates in cirrus clouds and GCM simulations, *Geophys. Res. Lett.*, *35*, L09806, doi:10.1029/2008GL033552.

Nakajima, T., and M. D. King (1990), Determination of the optical thickness and effective particle radius of clouds from reflected solar radiation measurements. Part I: Theory, *J. Atmos. Sci.*, *47*, 1878–1893.

Nasiri, S. L., and B. H. Kahn (2008), Limitations of bi-spectral infrared cloud phase determination and potential for improvement, *J. Appl. Meteorol. Climatol.*, *47*, 2895–2910.

Nasiri, S. L., V. T. Dang, B. H. Kahn, E. J. Fetzer, E. M. Manning, M. M. Schreier, and R. A. Frey (2011), Comparing MODIS and AIRS infrared-based cloud retrievals, *J. Appl. Meteorol. Climatol.*, *50*, 1057–1072, doi:10.1175/2010JAMC2603.1.

Naud, C. M., and B. H. Kahn (2015), Thermodynamic phase and ice cloud properties in northern hemisphere winter extratropical cyclones observed by Aqua AIRS, *J. Appl. Meteorol. Climatol.*, doi:10.1175/JAMC-D-15-0045.1, in press.

Niu, J., P. Yang, H.-L. Huang, J. E. Davies, J. Li, B. A. Baum, and Y. X. Hu (2007), A fast infrared radiative transfer model for overlapping clouds, *J. Quant. Spectrosc. Radiat. Transfer*, *103*, 447–459.

Platnick, S. (2000), Vertical photon transport in cloud remote sensing problems, *J. Geophys. Res.*, *105*, 22,919–22,935.

Platnick, S., M. D. King, S. A. Ackerman, W. P. Menzel, B. A. Baum, and R. A. Frey (2003), The MODIS cloud products: Algorithms and examples from Terra, *IEEE Trans. Geosci. Remote Sens.*, *41*, 459–473.

Platnick, S., et al. (2014), MODIS cloud optical properties: User guide for the collection 6 level-2 MOD06/MYD06 product and associated level-3 datasets, 116 pp. [Available at http://modisatmos.gsfc.nasa.gov/_docs/C6MOD06OPUserGuide.pdf.]

Posselt, D., T. S. L'Ecuyer, and G. L. Stephens (2008), Exploring the error characteristics of thin ice cloud property retrievals using a Markov chain Monte Carlo algorithm, *J. Geophys. Res.*, *113*, D24206, doi:10.1029/2008JD010832.

Riedi, J., B. Marchant, S. Platnick, B. A. Baum, F. Thieuleux, C. Oudard, F. Parol, J.-M. Nicolas, and P. Dubuisson (2010), Cloud thermodynamic phase inferred from merged POLDER and MODIS data, *Atmos. Chem. Phys.*, *10*, 11,851–11,865.

Rodgers, C. D. (2000), *Inverse Methods for Atmospheric Sounding: Theory and Practice*, 238 pp., World Sci., Singapore.

Rossow, W. B., et al. (1985), ISCCP cloud algorithm intercomparison, *J. Clim. Appl. Meteorol.*, *24*, 877–903.

Schreier, M. M., B. H. Kahn, A. Eldering, D. A. Elliott, E. Fishbein, F. W. Irion, and T. S. Pagano (2010), Radiance comparisons of MODIS and AIRS using spatial response information, *J. Atmos. Oceanic Technol.*, *27*, 1331–1342, doi:10.1175/2010JTECHA1424.1.

Stein, T. H. M., J. Delanoë, and R. J. Hogan (2011), A comparison among four different retrieval methods for ice-cloud properties using data from CloudSat, CALIPSO, and MODIS, *J. Appl. Meteorol. Climatol.*, *50*, 1952–1969.

Storelvmo, T., C. Hoose, and P. Eriksson (2011), Global modeling of mixed-phase clouds: The albedo and lifetime effects of aerosols, *J. Geophys. Res.*, *116*, D05207, doi:10.1029/2010JD014724.

Stubenrauch, C. J., et al. (2013), Assessment of global cloud datasets from satellites: Project and database initiated by the GEWEX radiation panel, *Bull. Am. Meteorol. Soc.*, *94*, 1031–1049, doi:10.1175/BAMS-D-12-00117.1.

Tsushima, Y., S. Emori, T. Ogura, M. Kimoto, M. J. Webb, K. D. Williams, M. A. Ringer, B. J. Soden, B. Li, and N. Andronova (2006), Importance of the mixed-phase cloud distribution in the control climate for assessing the response of clouds to carbon dioxide increase: A multi-model study, *Clim. Dyn.*, *27*, 113–126.

Waliser, D., et al. (2009), Cloud ice: A climate model challenge with signs and expectations of progress, *J. Geophys. Res.*, *114*, D00A21, doi:10.1029/2008JD010015.

Wang, C. (2013), Investigation of thin cirrus cloud optical and microphysical properties on the basis of satellite observations and fast radiative transfer models, PhD dissertation, 180 pp., Texas A&M Univ.

Wang, C., P. Yang, S. Platnick, A. K. Heidinger, B. A. Baum, T. Greenwald, Z. Zhang, and R. E. Holz (2013), Retrieval of ice cloud properties from AIRS and MODIS observations based on a fast high-spectral-resolution radiative transfer model, *J. Appl. Meteorol. Climatol.*, *52*, 710–726, doi:10.1175/JAMC-D-12-020.1.

Wei, H., P. Yang, J. Li, B. A. Baum, H. L. Huang, S. Platnick, Y. X. Hu, and L. Strow (2004), Retrieval of semitransparent ice cloud optical thickness from Atmospheric Infrared Sounder (AIRS) measurements, *IEEE Trans. Geosci. Remote Sens.*, *42*, 2254–2266.

Wind, G., S. Platnick, M. D. King, P. A. Hubanks, M. J. Pavolonis, A. K. Heidinger, P. Yang, and B. A. Baum (2010), Multilayer cloud detection with the MODIS near-infrared water vapor absorption band, *J. Appl. Meteorol. Climatol.*, *49*, 2315–2333, doi:10.1175/2010JAMC2364.1.

Zhang, Z., S. Platnick, P. Yang, A. K. Heidinger, and J. M. Comstock (2010), Effects of ice particle size vertical inhomogeneity on the passive remote sensing of ice clouds, *J. Geophys. Res.*, *115*, D17203, doi:10.1029/2010JD013835.